

# Optimal Linear Precoder Design for MIMO-OFDM Integrated Sensing and Communications Based on Bayesian Cramér-Rao Bound

Xinyang Li<sup>\*†</sup>, Vlad C. Andrei<sup>\*‡</sup>, Ullrich J. Mönich<sup>\*§</sup> and Holger Boche<sup>\*¶</sup>

<sup>\*</sup>Chair of Theoretical Information Technology, Technical University of Munich, Munich, Germany

<sup>\*</sup>BMBF Research Hub 6G-life, <sup>¶</sup>Munich Center for Quantum Science and Technology, <sup>¶</sup>Munich Quantum Valley

Email: <sup>†</sup>xinyang.li@tum.de, <sup>‡</sup>vlad.andrei@tum.de, <sup>§</sup>moenich@tum.de, <sup>¶</sup>boche@tum.de

**Abstract**—In this paper, we investigate the fundamental limits of MIMO-OFDM integrated sensing and communications (ISAC) systems based on a Bayesian Cramér-Rao bound (BCRB) analysis. We derive the BCRB for joint channel parameter estimation and data symbol detection, in which a performance trade-off between both functionalities is observed. We formulate the optimization problem for a linear precoder design and propose the stochastic Riemannian gradient descent (SRGD) approach to solve the non-convex problem. We analyze the optimality conditions and show that SRGD ensures convergence with high probability. The simulation results verify our analyses and also demonstrate a fast convergence speed. Finally, the performance trade-off is illustrated and investigated.

**Index Terms**—Integrated sensing and communications, MIMO-OFDM, Bayesian Cramér-Rao bound

## I. INTRODUCTION

With the increasing demand for massive device connection and high-speed communications, current wireless networks face many challenges, such as interference and spectrum sparsity. To overcome these problems, integrated sensing and communications (ISAC) is envisioned as a key technology in next-generation wireless systems [1]. Due to similar platform requirements and signal processing algorithms [2], it becomes more and more desirable to merge both functionalities to further explore performance potential and reduce hardware cost. Additionally, ISAC facilitates coordination between both functionalities through mutual assistance to improve individual performance such as accuracy, robustness, and security [3].

Multiple-input multiple-output (MIMO) and orthogonal frequency-division multiplexing (OFDM) are both powerful techniques that enable the efficient utilization of spectral and spatial resources. They have been standardized in most wireless systems such as Wi-Fi and 5G, and are still expected to be important signaling techniques in the next-generation systems, e.g., Beyond 5G and 6G [4]. Therefore, implementing ISAC in MIMO-OFDM systems is of great interest and is able

to be adopted in most applications, e.g., Internet of Things (IoT) [5] and perceptive mobile networks [6].

Waveform design plays a crucial role in ISAC systems as it directly impacts the theoretical system performance. Designing waveforms with favorable properties usually involves solving optimization problems that are formulated based on certain criteria. For example, the authors in [7] formulate the design problem to minimize the multi-user interference while maintaining the radar beampattern and peak to average power ratio (PAPR) constraints, and in [8], [9] the sensing symbols are designed and allocated to an OFDM grid to lower the Cramér-Rao bound (CRB) of sensing parameters. However, the fundamental limits for ISAC are still not well studied [10], due to the different performance requirements of both functionalities. Moreover, the formulated problems are usually non-convex and are therefore difficult to solve. In the cases where suboptimal solutions are targeted, convergence guarantees and the speed of the adopted algorithms are both critical factors to be considered.

In this work, we investigate the MIMO-OFDM ISAC performance from the perspective of Bayesian Cramér-Rao bound (BCRB), which generalizes the CRB by considering the prior distribution of parameters being estimated. In particular, we consider ISAC to be a task of joint channel parameter estimation and data symbol detection and derive its Bayesian Fisher information matrix (BFIM), the inverse of the BCRB. We point out the performance trade-off between both functionalities by taking the log determinant of the BFIM. Based on that, the optimization problem to design the linear precoder is formulated. We propose solving the non-convex stochastic problem using the stochastic Riemannian gradient descent (SRGD) method and prove that its convergence ensures the optimality conditions. Simulation results<sup>1</sup> highlight the advantages of SRGD and validate our analyses.

## II. SYSTEM MODEL

### A. Signal Model

We study a MIMO-OFDM system where the transmitter (Tx) and the receiver (Rx) each have a uniform linear array (ULA) with  $N_t$  and  $N_r$  antenna elements, respectively. The Tx

<sup>1</sup>Code is available at <https://github.com/xinyangli/isac-mimo-ofdm-wf>.

The authors were supported in part by the German Federal Ministry of Education and Research (BMBF) in the programme “Souverän. Digital. Vernetzt.” within the research hub 6G-life under Grant 16KISK002. U. Mönich and H. Boche were supported in part by the BMBF within the project “Post Shannon Communication - NewCom” under Grant 16KIS1003K.

allocates a set of  $M$  resource elements (REs)  $\{(n_m, k_m)\}_{m=1}^M$  for data transmission, in which we denote  $(n_m, k_m)$  as the index of the  $n_m$ -th subcarrier and the  $k_m$ -th OFDM symbol. These REs are filled with  $M$  unknown data symbols  $\mathbf{s}_m \in \mathbb{C}^{N_s}$  with  $N_s$  being the number of streams. We assume that the symbols follow a complex Gaussian distribution with zero mean and an identity covariance matrix, i.e.,  $\mathbf{s}_m \sim \mathcal{CN}(\mathbf{0}, \mathbf{I}_{N_s})$  for all  $m$ . By applying a linear precoder  $\mathbf{W} \in \mathbb{C}^{N_t \times N_s}$ , the data symbols are mapped to the  $N_t$  antennas via  $\mathbf{x}_m = \mathbf{W}\mathbf{s}_m$  for transmission, and the received signal after going through the channel can be expressed as [2]

$$\mathbf{y}_m = \mathbf{H}_m \mathbf{x}_m + \mathbf{z}_m, \quad (1)$$

where  $\mathbf{H}_m \in \mathbb{C}^{N_r \times N_t}$  is the channel matrix on the  $m$ -th RE and  $\mathbf{z}_m \in \mathbb{C}^{N_r}$  is complex white Gaussian noise following  $\mathcal{CN}(\mathbf{0}, \sigma_z^2 \mathbf{I}_{N_r})$  for all  $m$ . By considering the sparse propagation paths in the high frequency range [11], the channel matrix characterized by multipath parameters takes the form

$$\mathbf{H}_m(\boldsymbol{\xi}) = \sum_{l=1}^L b_l \omega_{m,l} \mathbf{a}_R(\phi_l) \mathbf{a}_T(\theta_l)^\top, \quad (2)$$

where  $\omega_{m,l} = e^{-j2\pi n_m f_0 \tau_l} e^{j2\pi f_{D,l} k_m T_s}$ ,  $f_0$  is the OFDM subcarrier spacing,  $T_s$  is the OFDM symbol duration,  $L$  is the number of propagation paths,  $b_l$ ,  $\tau_l$ ,  $f_{D,l}$ ,  $\theta_l$ ,  $\phi_l$  are the channel gain, path delay, Doppler shift, angle of departure (AoD) and angle of arrival (AoA) of the  $l$ -th path,  $\mathbf{a}_T(\cdot) \in \mathbb{C}^{N_t}$  and  $\mathbf{a}_R(\cdot) \in \mathbb{C}^{N_r}$  are the transmit and receive ULA response vector, respectively.  $\boldsymbol{\xi}$  contains all the multipath parameters and is defined as  $\boldsymbol{\xi} = [\mathbf{b}_R^\top, \mathbf{b}_I^\top, \boldsymbol{\tau}^\top, \mathbf{f}_D^\top, \boldsymbol{\theta}^\top, \boldsymbol{\phi}^\top]^\top \in \mathbb{R}^{6L}$ , with each component grouping the respective parameters of all  $L$  paths. To make  $\boldsymbol{\xi}$  a real vector, we split the path gains into real and imaginary parts and stack them into  $\mathbf{b}_R$  and  $\mathbf{b}_I$ .

As one of the scenarios in ISAC, the Rx aims to estimate channel parameters and detect data symbols jointly. Toward this goal, we utilize the BCRB [12], [13], which states a lower bound for the mean squared error (MSE) for any estimator.

### B. Bayesian Fisher Information Matrix

We stack the channel parameters and data symbols into a single vector as  $\boldsymbol{\zeta} = [\boldsymbol{\xi}^\top, \tilde{\mathbf{s}}_1^\top, \dots, \tilde{\mathbf{s}}_M^\top]^\top \in \mathbb{R}^{6L+2N_s M}$ , where  $\tilde{\mathbf{s}}_m = [\mathbf{s}_{m,R}^\top, \mathbf{s}_{m,I}^\top]^\top$ ,  $\mathbf{s}_m = \mathbf{s}_{m,R} + j\mathbf{s}_{m,I}$ . The ISAC system can then be considered as a system with input  $\boldsymbol{\zeta}$ , and output  $\mathbf{Y} = [\mathbf{y}_1, \mathbf{y}_2, \dots, \mathbf{y}_M]$  with the joint distribution

$$p(\mathbf{Y}, \boldsymbol{\zeta}) = p(\mathbf{Y}|\boldsymbol{\zeta})p(\boldsymbol{\zeta}) = p(\boldsymbol{\zeta}) \prod_{m=1}^M p(\mathbf{y}_m|\boldsymbol{\zeta}). \quad (3)$$

For any estimator  $\hat{\boldsymbol{\zeta}}(\mathbf{Y})$  of  $\boldsymbol{\zeta}$  and the resulting MSE, we have the BCRB as its lower bound, i.e.,

$$\mathbb{E} \left[ \left( \boldsymbol{\zeta} - \hat{\boldsymbol{\zeta}}(\mathbf{Y}) \right) \left( \boldsymbol{\zeta} - \hat{\boldsymbol{\zeta}}(\mathbf{Y}) \right)^\top \right] \succeq \mathcal{I}^{-1} \quad (4)$$

where  $\mathbf{A} \succeq \mathbf{B}$  indicates  $\mathbf{A} - \mathbf{B}$  is a positive semidefinite (PSD) matrix,  $\mathcal{I}$  is the BFIM and is defined as [14]

$$\mathcal{I} = \mathbb{E}_{\mathbf{Y}, \boldsymbol{\zeta}} \left[ \frac{\partial \log p(\mathbf{Y}, \boldsymbol{\zeta})}{\partial \boldsymbol{\zeta}} \left( \frac{\partial \log p(\mathbf{Y}, \boldsymbol{\zeta})}{\partial \boldsymbol{\zeta}} \right)^\top \right]. \quad (5)$$

By making use of (3), the BFIM can be decomposed into two parts, i.e.,

$$\mathcal{I} = \mathbb{E}_{\boldsymbol{\zeta}} [\mathcal{I}_c] + \mathcal{I}_p, \quad (6)$$

with  $\mathcal{I}_c$  and  $\mathcal{I}_p$  denoting the conditional and prior FIM respectively and taking the forms

$$\begin{aligned} \mathcal{I}_c &= \mathbb{E}_{\mathbf{Y}|\boldsymbol{\zeta}} \left[ \frac{\partial \log p(\mathbf{Y}|\boldsymbol{\zeta})}{\partial \boldsymbol{\zeta}} \left( \frac{\partial \log p(\mathbf{Y}|\boldsymbol{\zeta})}{\partial \boldsymbol{\zeta}} \right)^\top \right], \\ \mathcal{I}_p &= \mathbb{E}_{\boldsymbol{\zeta}} \left[ \frac{\partial \log p(\boldsymbol{\zeta})}{\partial \boldsymbol{\zeta}} \left( \frac{\partial \log p(\boldsymbol{\zeta})}{\partial \boldsymbol{\zeta}} \right)^\top \right]. \end{aligned} \quad (7)$$

We assume a Gaussian prior distribution  $p(\boldsymbol{\zeta}) = \mathcal{N}(\boldsymbol{\mu}_\zeta, \mathbf{C}_\zeta)$ , where  $\boldsymbol{\mu}_\zeta$  and  $\mathbf{C}_\zeta$  can be chosen practically. For instance, when the sequential estimation and tracking are applied, the prior mean of channel parameters  $\boldsymbol{\mu}_\xi$  can be set to the previous state, and their prior covariance matrix  $\mathbf{C}_\xi$  contains the uncertainty in them. Furthermore, we have  $\tilde{\mathbf{s}}_m$  following  $\mathcal{N}(\mathbf{0}, \frac{1}{2}\mathbf{I}_{2N_s})$ , and assume  $\tilde{\mathbf{s}}_m$  and  $\boldsymbol{\xi}$  are independent, such that  $\mathbf{C}_\zeta$  is a block diagonal matrix with  $\mathbf{C}_\xi$  and  $\frac{1}{2}\mathbf{I}_{2N_s}$  on the diagonal. The conditional distribution  $p(\mathbf{y}_m|\boldsymbol{\zeta})$  is a complex Gaussian distribution with mean  $\boldsymbol{\mu}_m = \mathbf{H}_m \mathbf{x}_m$  and covariance matrix  $\sigma_z^2 \mathbf{I}_{N_r}$ . Hence, we have [15]

$$\mathcal{I}_c = \frac{2}{\sigma_z^2} \sum_{m=1}^M \text{Re} \left( \frac{\partial \boldsymbol{\mu}_m^H}{\partial \boldsymbol{\zeta}} \frac{\partial \boldsymbol{\mu}_m}{\partial \boldsymbol{\zeta}} \right). \quad (8)$$

It can also be shown that [10]

$$\mathcal{I}_c = \begin{bmatrix} \mathcal{I}_c^s(\boldsymbol{\xi}, \boldsymbol{\xi}) & \mathcal{I}_c^s(\boldsymbol{\xi}, \tilde{\mathbf{s}}_1) & \cdots & \mathcal{I}_c^s(\boldsymbol{\xi}, \tilde{\mathbf{s}}_M) \\ \mathcal{I}_c^s(\tilde{\mathbf{s}}_1, \boldsymbol{\xi}) & \mathcal{I}_c^s(\tilde{\mathbf{s}}_1, \tilde{\mathbf{s}}_1) & \cdots & \mathcal{I}_c^s(\tilde{\mathbf{s}}_1, \tilde{\mathbf{s}}_M) \\ \vdots & \vdots & \ddots & \vdots \\ \mathcal{I}_c^s(\tilde{\mathbf{s}}_M, \boldsymbol{\xi}) & \mathcal{I}_c^s(\tilde{\mathbf{s}}_M, \tilde{\mathbf{s}}_1) & \cdots & \mathcal{I}_c^s(\tilde{\mathbf{s}}_M, \tilde{\mathbf{s}}_M) \end{bmatrix} \quad (9)$$

with the arguments inside the bracket of the submatrix  $\mathcal{I}_c^s(\cdot, \cdot)$  denoting to which components of  $\boldsymbol{\zeta}$  the derivatives in (8) are taken. In [9] it is derived that

$$\frac{\partial \boldsymbol{\mu}_m}{\partial \boldsymbol{\xi}} = (\mathbf{R}\boldsymbol{\Lambda}_m) * (\mathbf{x}_m^\top \mathbf{T}) \quad (10)$$

$$\mathcal{I}_c^s(\boldsymbol{\xi}, \boldsymbol{\xi}) = \frac{2}{\sigma_z^2} \sum_{m=1}^M \text{Re} \left( \boldsymbol{\Lambda}_m^H \mathbf{T}^H \mathbf{x}_m^* \mathbf{x}_m^\top \mathbf{T} \boldsymbol{\Lambda}_m \circ (\mathbf{R}^H \mathbf{R}) \right), \quad (11)$$

where we define  $*$  and  $\circ$  as the Khatri-Rao product and the Hadamard product, respectively, and the related matrices are given in (14). In addition,

$$\frac{\partial \boldsymbol{\mu}_m}{\partial \tilde{\mathbf{s}}_{m'}} = \begin{cases} \begin{bmatrix} \mathbf{H}_m & \mathbf{H}_m \end{bmatrix} \begin{bmatrix} \mathbf{W} \\ j\mathbf{W} \end{bmatrix} = \tilde{\mathbf{H}}_m \tilde{\mathbf{W}}, & m = m' \\ \mathbf{0}, & m \neq m' \end{cases} \quad (12)$$

$$\mathcal{I}_c^s(\tilde{\mathbf{s}}_m, \tilde{\mathbf{s}}_m) = \frac{2}{\sigma_z^2} \text{Re} \left( \tilde{\mathbf{W}}^H \tilde{\mathbf{H}}_m^H \tilde{\mathbf{H}}_m \tilde{\mathbf{W}} \right) \quad (13)$$

$$\begin{aligned}
\Lambda_m &= \text{blkdiag} \{ \Omega_m, j\Omega_m, \mathbf{G}_m \mathbf{B}, \mathbf{F}_m \mathbf{B}, \Omega_m \mathbf{B}, \Omega_m \mathbf{B} \}, \quad \mathbf{B} = \text{diag} \{ b_1 \cdots b_L \}, \quad \Omega_m = \text{diag} \{ \omega_{m,1} \cdots \omega_{m,L} \} \\
\mathbf{G}_m &= \text{diag} \{ u_{m,1} \cdots u_{m,L} \}, \quad \mathbf{F}_m = \text{diag} \{ v_{m,1} \cdots v_{m,L} \}, \quad u_{m,l} = \frac{\partial \omega_{m,l}}{\partial \tau_l} = -j2\pi n f_0 \omega_{m,l}, \quad v_{m,l} = \frac{\partial \omega_{m,l}}{\partial f_{D,l}} = j2\pi k T_s \omega_{m,l}, \\
\mathbf{T} &= [\mathbf{A}_T, \mathbf{A}_T, \mathbf{A}_T, \mathbf{A}_T, \mathbf{A}_T, \mathbf{D}_T], \quad \mathbf{A}_T = [\mathbf{a}_T(\theta_1) \cdots \mathbf{a}_T(\theta_L)], \quad \mathbf{D}_T = [\mathbf{d}_T(\theta_1) \cdots \mathbf{d}_T(\theta_L)], \quad \mathbf{d}_T(\theta_l) = \frac{\partial \mathbf{a}_T(\theta_l)}{\partial \theta_l}, \\
\mathbf{R} &= [\mathbf{A}_R, \mathbf{A}_R, \mathbf{A}_R, \mathbf{A}_R, \mathbf{D}_R, \mathbf{A}_R], \quad \mathbf{A}_R = [\mathbf{a}_R(\phi_1) \cdots \mathbf{a}_R(\phi_L)], \quad \mathbf{D}_R = [\mathbf{d}_R(\phi_1) \cdots \mathbf{d}_R(\phi_L)], \quad \mathbf{d}_R(\phi_l) = \frac{\partial \mathbf{a}_R(\phi_l)}{\partial \phi_l}.
\end{aligned} \tag{14}$$

Therefore, taking the expectation with respect to each component in (9) leads to

$$\begin{aligned}
&\mathbb{E}_\zeta [\mathcal{I}_c^s(\boldsymbol{\xi}, \boldsymbol{\xi})] \\
&= \frac{2}{\sigma_z^2} \sum_{m=1}^M \mathbb{E}_\xi [\text{Re} (\Lambda_m^H \mathbf{T}^H \mathbb{E}_{s_m} [\mathbf{x}_m^* \mathbf{x}_m^T] \mathbf{T} \Lambda_m) \circ (\mathbf{R}^H \mathbf{R})] \\
&= \frac{2}{\sigma_z^2} \sum_{m=1}^M \mathbb{E}_\xi \left[ \underbrace{\text{Re} (\Lambda_m^H \mathbf{T}^H \mathbf{W}^* \mathbf{W}^T \mathbf{T} \Lambda_m) \circ (\mathbf{R}^H \mathbf{R})}_{S_m(\mathbf{W}, \boldsymbol{\xi})} \right],
\end{aligned} \tag{15}$$

$$\begin{aligned}
&\mathbb{E}_\zeta [\mathcal{I}_c^s(\tilde{s}_m, \tilde{s}_{m'})] \\
&= \begin{cases} \frac{2}{\sigma_z^2} \text{Re} \left( \tilde{\mathbf{W}}^H \mathbb{E}_\xi \left[ \tilde{\mathbf{H}}_m^H \tilde{\mathbf{H}}_m \right] \tilde{\mathbf{W}} \right), & m = m' \\ \mathbf{0}, & m \neq m', \end{cases}
\end{aligned} \tag{16}$$

$$\begin{aligned}
&\mathbb{E}_\zeta [\mathcal{I}_c^s(\boldsymbol{\xi}, \tilde{s}_m)] \\
&= \frac{2}{\sigma_z^2} \sum_{m=1}^M \mathbb{E}_\zeta \left[ \text{Re} \left( (\mathbf{R} \Lambda_m) * (\mathbf{x}_m^T \mathbf{T}) \tilde{\mathbf{H}}_m \tilde{\mathbf{W}} \right) \right] \\
&= \mathbf{0},
\end{aligned} \tag{17}$$

where the last step is due to the mean of  $\mathbf{x}_m$  being zero. The second term  $\mathcal{I}_p$  is straightforward to be obtained as

$$\mathcal{I}_p = \mathbf{C}_\zeta^{-1} = \begin{bmatrix} \mathbf{C}_\xi^{-1} & \mathbf{0} \\ \mathbf{0} & 2\mathbf{I}_{2N_s M} \end{bmatrix}. \tag{18}$$

Consequently, the BFIM is a block diagonal matrix with nonzero matrices  $\mathbb{E}_\zeta [\mathcal{I}_c^s(\boldsymbol{\xi}, \boldsymbol{\xi})] + \mathbf{C}_\xi^{-1}$  and  $\mathbb{E}_\zeta [\mathcal{I}_c^s(\tilde{s}_m, \tilde{s}_m)] + 2\mathbf{I}_{2N_s}$  for all  $m$  on the diagonal.

### III. PROBLEM FORMULATION

The BFIM can be optimized using different criteria [16]. In this work, we choose the log determinant as the objective function, which results in

$$\begin{aligned}
\log \det (\mathcal{I}) &= \log \det \left( \mathbb{E}_\zeta [\mathcal{I}_c^s(\boldsymbol{\xi}, \boldsymbol{\xi})] + \mathbf{C}_\xi^{-1} \right) \\
&+ \sum_{m=1}^M \log \det \left( \mathbb{E}_\zeta [\mathcal{I}_c^s(\tilde{s}_m, \tilde{s}_m)] + 2\mathbf{I}_{2N_s} \right).
\end{aligned} \tag{19}$$

By plugging the expression of  $\mathbb{E}_\zeta [\mathcal{I}_c^s(\tilde{s}_m, \tilde{s}_m)]$  from (16) into the second term, we have

$$\begin{aligned}
&\log \det \left( \mathbb{E}_\zeta [\mathcal{I}_c^s(\tilde{s}_m, \tilde{s}_m)] + 2\mathbf{I}_{2N_s} \right) \\
&= \log \det \left( \frac{2}{\sigma_z^2} \text{Re} \left( \tilde{\mathbf{W}}^H \mathbb{E}_\xi \left[ \tilde{\mathbf{H}}_m^H \tilde{\mathbf{H}}_m \right] \tilde{\mathbf{W}} \right) + 2\mathbf{I}_{2N_s} \right) \\
&= \log \det \left( \text{Re} \left( \begin{bmatrix} \mathbf{A} + 2\mathbf{I}_{N_s} & j\mathbf{A} \\ -j\mathbf{A} & \mathbf{A} + 2\mathbf{I}_{N_s} \end{bmatrix} \right) \right) \\
&= \log \det \left( \begin{bmatrix} \text{Re}(\mathbf{A} + 2\mathbf{I}_{N_s}) & -\text{Im}(\mathbf{A} + 2\mathbf{I}_{N_s}) \\ \text{Im}(\mathbf{A} + 2\mathbf{I}_{N_s}) & \text{Re}(\mathbf{A} + 2\mathbf{I}_{N_s}) \end{bmatrix} \right) \\
&= 2 \log \det (\mathbf{A} + 2\mathbf{I}_{N_s}) \\
&= 2 \log \det \left( \frac{2}{\sigma_z^2} \mathbf{W}^H \mathbb{E}_\xi [\mathbf{H}_m^H \mathbf{H}_m] \mathbf{W} + 2\mathbf{I}_{N_s} \right),
\end{aligned} \tag{20}$$

with  $\mathbf{A} = \frac{2}{\sigma_z^2} \mathbf{W}^H \mathbb{E}_\xi [\mathbf{H}_m^H \mathbf{H}_m] \mathbf{W}$ . It's not surprising that (20) has a similar form with the mutual information between  $s_m$  and  $\mathbf{y}_m$ . In fact, if we omit the factor 2 inside and outside the log det, (20) is an upper bound on the ergodic mutual information between  $s_m$  with  $\mathbf{y}_m$ , since

$$\begin{aligned}
\mathbb{E}_\xi [I(s_m, \mathbf{y}_m)] &= \mathbb{E}_\xi \left[ \log \det \left( \frac{1}{\sigma_z^2} \mathbf{W}^H \mathbf{H}_m^H \mathbf{H}_m \mathbf{W} + \mathbf{I}_{N_s} \right) \right] \\
&\leq \log \det \left( \frac{1}{\sigma_z^2} \mathbf{W}^H \mathbb{E}_\xi [\mathbf{H}_m^H \mathbf{H}_m] \mathbf{W} + \mathbf{I}_{N_s} \right)
\end{aligned} \tag{21}$$

using the Jensen inequality, and  $I(\cdot, \cdot)$  denotes the mutual information. The first term in (19) is nothing else than the log det of the BFIM for channel parameter estimation. Therefore, we observe a performance trade-off between both functionalities in which the communication quality is measured in terms of the upper bound of the ergodic mutual information, channel sensing is assessed by the parameter estimation error bound, and both are bridged through the BCRB of joint parameter estimation and symbol detection. By introducing an adjustable weighting factor to (19), we are able to take over the control of such a trade-off while optimizing.

We also take into consideration different importance levels of different channel parameters in practice. To do this, we multiply the BFIM for the parameter part by a weighting matrix  $\mathbf{J}$  [16]. Therefore, the resulting optimization problem

based on (19) is formulated as

$$\begin{aligned}
\max_{\mathbf{W}} f(\mathbf{W}; \alpha) &= \max_{\mathbf{W}} \alpha f_s(\mathbf{W}) + (1 - \alpha) \frac{1}{M} f_c(\mathbf{W}) \\
&= \max_{\mathbf{W}} \alpha \log \det \left( \mathbf{J}^H \left( \frac{2}{\sigma_z^2} \sum_{m=1}^M \mathbb{E}_{\xi} [\mathbf{S}_m(\mathbf{W}, \xi)] + \mathbf{C}_{\xi}^{-1} \right) \mathbf{J} \right) \\
&\quad + \frac{1 - \alpha}{M} \sum_{m=1}^M 2 \log \det \left( \frac{2}{\sigma_z^2} \mathbf{W}^H \mathbb{E}_{\xi} [\mathbf{H}_m^H \mathbf{H}_m] \mathbf{W} + 2\mathbf{I} \right) \\
\text{s. t.} \quad \text{tr}(\mathbf{W}\mathbf{W}^H) &= \|\mathbf{W}\|_F^2 \leq P,
\end{aligned} \tag{P1}$$

with  $\alpha \in [0, 1]$  the trade-off factor,  $\mathbf{S}_m(\mathbf{W}, \xi)$  given in (15), and  $f_s(\mathbf{W})$ ,  $f_c(\mathbf{W})$  indicating performance metrics for sensing and communications, respectively. To scale both quantities to the same order,  $f_c(\mathbf{W})$  is multiplied by  $\frac{1}{M}$ . Such a problem is difficult to solve for two reasons. The first one is that the expectation in the objective function is intractable to derive. The stochastic optimization methods [17] can be applied in which the expectation is approximated by sampling  $\xi$  from the prior distribution, as will be discussed later. The other reason is that it is a non-convex problem if  $\mathbf{W}$  is a tall matrix, i.e.,  $N_s < N_t$ . This issue can be addressed partly by semidefinite relaxation (SDR) [18], but as  $N_t$  and the number of sampling points become larger, SDR suffers from higher computational costs and becomes infeasible to solve in practice [9]. To this end, we observe that  $f(\mathbf{W}; \alpha)$  is maximized only if the transmit power  $P$  is exhausted due to the monotonicity of  $f$  in the scaling of  $\mathbf{W}$ , which leads to the complex hypersphere manifold

$$\mathcal{S} = \{ \mathbf{W} \in \mathbb{C}^{N_t \times N_s} \mid \text{tr}(\mathbf{W}\mathbf{W}^H) = P \}. \tag{22}$$

Hence, (P1) can be solved using Riemannian manifold optimization methods [19] on  $\mathcal{S}$ . Taking into account the stochastic approximation and defining

$$\begin{aligned}
\mathbf{S}_m^N(\mathbf{W}) &= \frac{1}{N} \sum_{n=1}^N \mathbf{S}_m(\mathbf{W}, \xi_n) \approx \mathbb{E}_{\xi} [\mathbf{S}_m(\mathbf{W}, \xi)] \\
\mathbf{K}_m^N &= \frac{1}{N} \sum_{n=1}^N \mathbf{H}_m(\xi_n)^H \mathbf{H}_m(\xi_n) \approx \mathbb{E}_{\xi} [\mathbf{H}_m^H \mathbf{H}_m],
\end{aligned} \tag{23}$$

with  $N$  the number of sampling points, and  $\xi_n$  the  $n$ -th sampled channel parameters, we end up with the final stochastic Riemannian manifold optimization (SRMO) problem

$$\begin{aligned}
\max_{\mathbf{W} \in \mathcal{S}} \hat{f}(\mathbf{W}; \alpha) &= \max_{\mathbf{W}} \alpha \hat{f}_s(\mathbf{W}) + (1 - \alpha) \frac{1}{M} \hat{f}_c(\mathbf{W}) \\
&= \max_{\mathbf{W} \in \mathcal{S}} \alpha \log \det \left( \mathbf{J}^H \left( \frac{2}{\sigma_z^2} \sum_{m=1}^M \mathbf{S}_m^N(\mathbf{W}) + \mathbf{C}_{\xi}^{-1} \right) \mathbf{J} \right) \\
&\quad + \frac{1 - \alpha}{M} \sum_{m=1}^M 2 \log \det \left( \frac{2}{\sigma_z^2} \mathbf{W}^H \mathbf{K}_m^N \mathbf{W} + 2\mathbf{I} \right)
\end{aligned} \tag{PM}$$

where we use  $\hat{(\cdot)}$  to indicate the stochastic version of a function. (PM) can be solved efficiently by applying SRGD.

In the following, we analyze the optimality conditions for the formulated problems and show that SRGD ensures the convergence to a critical point of (P1).

#### IV. OPTIMIZATION

To state the optimality conditions for the constrained problems above, we define the Lagrangian function as

$$\mathcal{L}(\mathbf{W}, \lambda) = -f(\mathbf{W}; \alpha) + \lambda (\text{tr}(\mathbf{W}\mathbf{W}^H) - P), \tag{24}$$

with  $\lambda$  being the Lagrangian multiplier. Let  $\nabla$  denote the complex gradient [20] in the Euclidean space, if we replace the power constraint in (P1) with equality, we have the following first-order optimality conditions [21]:

**Theorem 1** (First-Order Necessary Conditions). *If  $\mathbf{W}_{\text{opt}}$  is a local optimum of (P1), then there exists a Lagrangian multiplier  $\lambda_{\text{opt}}$  such that*

$$\nabla \mathcal{L}(\mathbf{W}_{\text{opt}}, \lambda_{\text{opt}}) = \mathbf{0}, \tag{25}$$

$$\text{tr}(\mathbf{W}_{\text{opt}} \mathbf{W}_{\text{opt}}^H) - P = 0. \tag{26}$$

Theorem 1 is also known as the Karush–Kuhn–Tucker (KKT) conditions. By plugging (24) into (25), we have

$$\nabla \mathcal{L}(\mathbf{W}_{\text{opt}}, \lambda_{\text{opt}}) = -\nabla f(\mathbf{W}_{\text{opt}}; \alpha) + 2\lambda_{\text{opt}} \mathbf{W}_{\text{opt}} = \mathbf{0}. \tag{27}$$

The principle of the Riemannian gradient method is similar to its Euclidean version. At the  $t$ -th iteration, the Riemannian gradient of  $f$  at  $\mathbf{W}_t$  is given as<sup>2</sup>

$$\text{grad} f(\mathbf{W}_t; \alpha) = \mathcal{P}_{\mathbf{W}_t}(\nabla f(\mathbf{W}_t; \alpha)), \tag{28}$$

where  $\mathcal{P}_{\mathbf{W}_t}(\cdot)$  is the projection operator that projects a vector in the Euclidean space onto the tangent space of  $\mathcal{S}$  at point  $\mathbf{W}_t$ . The update function moves  $\mathbf{W}_t$  along the direction of  $\text{grad} f(\mathbf{W}_t; \alpha)$  or its variants to the next point  $\mathbf{W}_{t+1} \in \mathcal{S}$ , which is performed by either exponential map or retraction, and the step size can be determined by any line search approach [19]. In particular, for the complex hypersphere, the projector is defined as

$$\mathcal{P}_{\mathbf{W}}(\mathbf{V}) = \mathbf{V} - \text{Re}(\text{tr}(\mathbf{W}^H \mathbf{V})) \mathbf{W}. \tag{29}$$

When  $\text{grad} f(\mathbf{W}; \alpha)$  converges to  $\mathbf{0}$ , we have

$$\nabla f(\mathbf{W}; \alpha) - \text{Re}(\text{tr}(\mathbf{W}^H \nabla f(\mathbf{W}; \alpha))) \mathbf{W} = \mathbf{0}, \tag{30}$$

and notice that it satisfies the KKT conditions. Hence, we have the following corollary:

**Corollary 1.** *If the Riemannian gradient of  $f$  at  $\mathbf{W}_{\text{opt}}$  vanishes, i.e.,  $\text{grad} f(\mathbf{W}_{\text{opt}}; \alpha) = \mathbf{0}$ ,  $\mathbf{W}_{\text{opt}}$  satisfies Theorem 1 with the Lagrangian multiplier being*

$$\lambda_{\text{opt}} = \frac{1}{2} \text{Re}(\text{tr}(\mathbf{W}_{\text{opt}}^H \nabla f(\mathbf{W}_{\text{opt}}; \alpha))). \tag{31}$$

*Proof.* By comparing (27) and (30) the result is obvious.  $\square$

Considering the SRGD for (PM), the following theorem [22] guarantees its convergence with high probability:

<sup>2</sup>Note that we use  $\text{grad}$  to denote the Riemannian gradient while  $\nabla$  indicates the Euclidean gradient.

**Theorem 2.** Suppose that the SRGD applied on (PM) generates a sequence of points  $\{\mathbf{W}_t\}_{t>0}$  and a sequence of step sizes  $\{\gamma_t\}_{t>0}$  satisfying  $\sum \gamma_t^2 < \infty$  and  $\sum \gamma_t = +\infty$ . The resulting sequence of the Riemannian gradients of  $f$  converges almost sure (a.s.), i.e.,  $\text{grad}f(\mathbf{W}_t; \alpha) \rightarrow \mathbf{0}$  a.s.. This holds true for either exponential map or retraction that is used as the update function.

*Proof.* See [22].  $\square$

The step size assumption in Theorem 2 is widely used as a sufficient condition for the convergence analysis in stochastic programming [23]. In simulations, we employ an adaptive line search method [24] to determine the step size at each iteration. Although it is challenging to verify the validity of the assumption on adaptive step size, our numerical results demonstrate that the proposed method can still converge reliably and rapidly.

Based on the above analyses, we can conclude that the solution of SRGD will converge to a KKT point of (P1) satisfying Theorem 1 a.s.. In addition, the stochastic nature enables the use of a small batch size of points sampled at each iteration, thereby reducing the computational complexity.

## V. NUMERICAL RESULTS

Throughout the simulations, the system settings are chosen as  $N_t = N_r = 8$ ,  $N_s = 3$ ,  $f_0 = 15$  kHz and a rectangular  $128 \times 14$  OFDM grid is allocated for data transmission, i.e.,  $n_m = 0 \dots 127$ ,  $k_m = 0 \dots 13$ . We perform the Monte Carlo approaches, and at each simulation the channel parameters  $\xi$  are randomly generated. In particular, we set the number of propagation paths to 3 and each parameter component is sampled according to the following rules: for all  $l$ ,  $b_l$  is sampled from the complex Gaussian distribution with zero mean and unit variance; the path distance is sampled uniformly from 10 to 800 meters based on which  $\tau_l$  is calculated; the relative velocity is sampled uniformly from 0 to 80 m/s on which  $f_{D,l}$  is calculated;  $\phi_l$  and  $\theta_l$  are both sampled uniformly from  $-90^\circ$  to  $90^\circ$ ; all components in  $\xi$  are independent of each other. The sampled parameter vector is also used as the prior mean  $\mu_\xi$  and the prior covariance  $\mathbf{C}_\xi$  is a diagonal matrix with the standard deviations for each type of parameter as follows:  $10^{-1}$  for path gains,  $10^{-7}$  for path delays, 50 for Doppler shifts,  $10^{-1}$  for AoAs and AoDs. The scaling matrix  $\mathbf{J}$  in  $f_s(\mathbf{W})$  is a diagonal matrix with diagonal elements being  $1/f_0$  and  $f_0$  for the delay and Doppler parts respectively, and 1 otherwise, in order to scale the values to a similar order and avoid numerical instability.

We first fix the trade-off factor  $\alpha$  to 0.5 and perform the stochastic Riemannian conjugate gradient (SRCG) method, a variant of SRGD, on (PM) for different numbers of samples per iteration  $N$ . The maximum number of iterations is set to 50 and the convergence of objective values averaged over all simulations are plotted in Fig. 1. It shows that SRGD converges quickly within 10 iterations. As  $N$  becomes larger, the curve converges to a lower value, but the performance improvement is not significant as  $N > 10$ . To validate

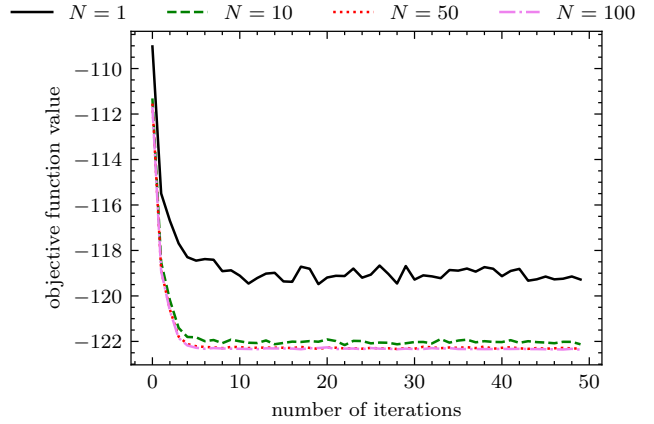


Fig. 1: Convergence of  $-\hat{f}(\mathbf{W}; \alpha)$  for different numbers of samples per iteration.

the gradient convergence, the evolution of the Riemannian gradient norms during optimization is illustrated in Fig. 2. In addition, their standard deviations over simulations are drawn in shadow. It turns out that for a larger  $N$ , the Riemannian gradient can converge to  $\mathbf{0}$  a.s.. The above results highlight the remarkable performance of SRGD in practice, especially its fast convergence and low demand for sample size per iteration.

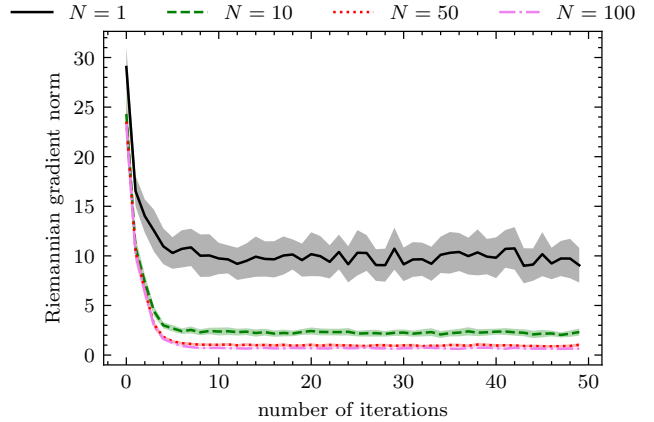


Fig. 2: Riemannian gradient norm convergence for different numbers of samples per iteration. The standard deviations over all simulations are drawn in shadow.

Based on the optimized precoders, we calculate the values of  $\hat{f}_s(\mathbf{W})$  and  $\hat{f}_c(\mathbf{W})$  on 100 samples and present their trade-off in Fig. 3 by varying the factor  $\alpha$ . The curves exhibit a similar behavior to the rate region for two-user MIMO systems [25], and their interior regions correspond to the achievable ISAC performance. In contrast to the case of designing waveform for communications and sensing separately, in which the curve will become a straight line connecting the achievable maximum  $\hat{f}_s(\mathbf{W})$  and maximum  $\hat{f}_c(\mathbf{W})$  [26], the Pareto boundary of the curves in Fig. 3 toward the upper right corner highlights the integration benefits gained by joint design.

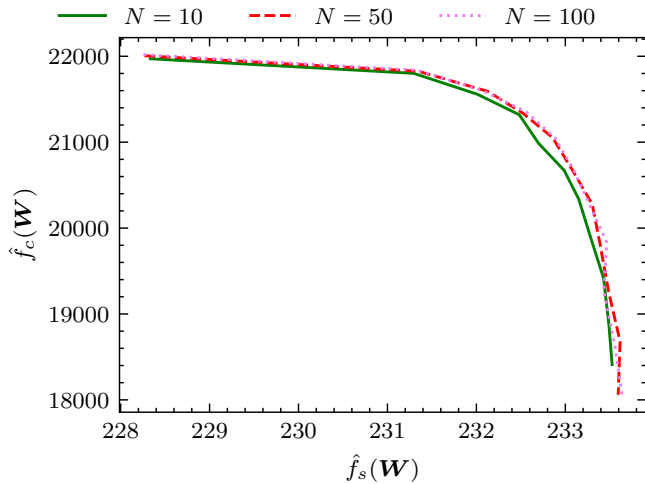


Fig. 3: Trade-off between the performance of communications and sensing while varying  $\alpha$  from 0 to 1.

## VI. CONCLUSION

In this work, we address the linear precoder design problem for MIMO-OFDM ISAC systems by optimizing the BFIM of channel parameters and data symbols. The proposed SRGD method is shown to guarantee a fast convergence with high probability. In addition, the derived objective function can be decomposed into two parts that correspond to the respective communication and sensing criteria., thereby making it possible to control the performance trade-off through a single factor. Furthermore, the performance achieved by the designed precoder is shown to be characterized by a Pareto boundary, indicating the benefits of joint system design. This observation motivates us to envision the BFIM as a potential unified metric for ISAC and we leave the further investigation and study as our future work.

## REFERENCES

- [1] F. Liu, Y. Cui, C. Masouros, J. Xu, T. X. Han, Y. C. Eldar, and S. Buzzi, "Integrated sensing and communications: Toward dual-functional wireless networks for 6G and beyond," *IEEE Journal on Selected Areas in Communications*, vol. 40, no. 6, pp. 1728–1767, 2022.
- [2] J. A. Zhang, F. Liu, C. Masouros, R. W. Heath, Z. Feng, L. Zheng, and A. Petropulu, "An overview of signal processing techniques for joint communication and radar sensing," *IEEE Journal of Selected Topics in Signal Processing*, vol. 15, no. 6, pp. 1295–1315, 2021.
- [3] H. M. Furqan, M. S. J. Solaija, H. Türkmen, and H. Arslan, "Wireless communication, sensing, and rem: A security perspective," *IEEE Open Journal of the Communications Society*, vol. 2, pp. 287–321, 2021.
- [4] P. Schwentek, G. T. Nguyen, H. Boche, W. Kellerer, and F. H. P. Fitzek, "6G perspective of mobile network operators, manufacturers, and verticals," *IEEE Networking Letters*, pp. 1–1, 2023.
- [5] S. He, K. Shi, C. Liu, B. Guo, J. Chen, and Z. Shi, "Collaborative sensing in internet of things: A comprehensive survey," *IEEE Communications Surveys & Tutorials*, vol. 24, no. 3, pp. 1435–1474, 2022.
- [6] M. L. Rahman, J. A. Zhang, X. Huang, Y. J. Guo, and R. W. Heath, "Framework for a perceptive mobile network using joint communication and radar sensing," *IEEE Transactions on Aerospace and Electronic Systems*, vol. 56, no. 3, pp. 1926–1941, 2020.
- [7] X. Hu, C. Masouros, F. Liu, and R. Nissel, "Low-PAPR DFRC MIMO-OFDM waveform design for integrated sensing and communications," in *ICC 2022 - IEEE International Conference on Communications*, 2022, pp. 1599–1604.

- [8] S. D. Liyanaarachchi, T. Riihonen, C. B. Barneto, and M. Valkama, "Optimized waveforms for 5G–6G communication with sensing: Theory, simulations and experiments," *IEEE Transactions on Wireless Communications*, vol. 20, no. 12, pp. 8301–8315, 2021.
- [9] X. Li, V. C. Andrei, U. Mönich, and H. Boche, "Optimal and robust waveform design for MIMO-OFDM channel sensing: A Cramér-Rao bound perspective," in *2023 IEEE International Conference on Communications (ICC): SAC Integrated Sensing and Communication Track (IEEE ICC'23 - SAC-13 ISAC Track)*, Rome, Italy, May 2023.
- [10] A. Liu, Z. Huang, M. Li, Y. Wan, W. Li, T. X. Han, C. Liu, R. Du, D. K. P. Tan, J. Lu, Y. Shen, F. Colone, and K. Chetty, "A survey on fundamental limits of integrated sensing and communication," *IEEE Communications Surveys & Tutorials*, vol. 24, no. 2, pp. 994–1034, 2022.
- [11] R. W. Heath, N. González-Prelcic, S. Rangan, W. Roh, and A. M. Sayeed, "An overview of signal processing techniques for millimeter wave MIMO systems," *IEEE Journal of Selected Topics in Signal Processing*, vol. 10, no. 3, pp. 436–453, 2016.
- [12] P. Tichavsky, C. Muravchik, and A. Nehorai, "Posterior Cramér-Rao bounds for discrete-time nonlinear filtering," *IEEE Transactions on Signal Processing*, vol. 46, no. 5, pp. 1386–1396, 1998.
- [13] H. L. Van Trees and K. L. Bell, "Bayesian bounds for parameter estimation and nonlinear filtering/tracking," *AMC*, vol. 10, no. 12, pp. 10–1109, 2007.
- [14] A. Vosoughi and A. Scaglione, "On the effect of receiver estimation error upon channel mutual information," *IEEE Transactions on Signal Processing*, vol. 54, no. 2, pp. 459–472, 2006.
- [15] S. M. Kay, *Fundamentals of statistical signal processing: estimation theory*. Prentice-Hall, Inc., 1993.
- [16] J. Li, L. Xu, P. Stoica, K. W. Forsythe, and D. W. Bliss, "Range compression and waveform optimization for MIMO radar: A Cramér-Rao bound based study," *IEEE Transactions on Signal Processing*, vol. 56, no. 1, pp. 218–232, 2008.
- [17] L. A. Hannah, "Stochastic optimization," *International Encyclopedia of the Social & Behavioral Sciences*, vol. 2, pp. 473–481, 2015.
- [18] Z.-q. Luo, W.-k. Ma, A. M.-c. So, Y. Ye, and S. Zhang, "Semidefinite relaxation of quadratic optimization problems," *IEEE Signal Processing Magazine*, vol. 27, no. 3, pp. 20–34, 2010.
- [19] P.-A. Absil, R. Mahony, and R. Sepulchre, "Optimization algorithms on matrix manifolds," in *Optimization Algorithms on Matrix Manifolds*. Princeton University Press, 2009.
- [20] K. B. Petersen, M. S. Pedersen *et al.*, "The matrix cookbook," *Technical University of Denmark*, vol. 7, no. 15, p. 510, 2008.
- [21] S. Wright, J. Nocedal *et al.*, "Numerical optimization," *Springer Science*, vol. 35, no. 67–68, p. 7, 1999.
- [22] S. Bonnabel, "Stochastic gradient descent on Riemannian manifolds," *IEEE Transactions on Automatic Control*, vol. 58, no. 9, pp. 2217–2229, 2013.
- [23] L. Leon Bottou, "Online learning and stochastic approximations," *Online learning in neural networks*, vol. 17, no. 9, p. 142, 1998.
- [24] N. Boumal, *An introduction to optimization on smooth manifolds*. Cambridge University Press, 2023. [Online]. Available: <https://www.nicolasboumal.net/book>
- [25] E. Biglieri, R. Calderbank, A. Constantinides, A. Goldsmith, A. Paulraj, and H. V. Poor, *MIMO wireless communications*. Cambridge university press, 2007.
- [26] Y. Xiong, F. Liu, Y. Cui, W. Yuan, T. X. Han, and G. Caire, "On the fundamental tradeoff of integrated sensing and communications under gaussian channels," *arXiv preprint arXiv:2204.06938*, 2022.